Computers and Mathematics with Applications 67 (2014) 350–362

Contents lists available at ScienceDirect

Computers and Mathematics with Applications

journal homepage: www.elsevier.com/locate/camwa

Multiphase cascaded lattice Boltzmann method☆

Daniel Lycett-Brown*, Kai H. Luo

Energy Technology Research Group, Faculty of Engineering and the Environment, University of Southampton, Southampton, SO17 1BJ, UK

ARTICLE INFO

Keywords:
Lattice Boltzmann
Cascaded LBM
Multiphase
Spurious velocities

ABSTRACT

To improve the stability of the lattice Boltzmann method (LBM) at high Reynolds number the cascaded LBM has recently been introduced. As in the multiple relaxation time (MRT) method the cascaded LBM introduces additional relaxation times into the collision operator, but does so in a co-moving reference frame. This has been shown to significantly increase stability at low viscosity in the single phase case. Here the cascaded LBM is further developed to include multiphase flow. For this the force term is calculated by the interaction potential method, and introduced into the collision operator via the exact difference method (EDM). Comparisons are made with the lattice Bhatnagar–Gross–Krook (LBGK) method, and an MRT implementation. Both the cascaded and MRT methods are shown to significantly reduce spurious velocities over the LBGK method. For the particular case of the Shan–Chen interparticle force term calculation with the EDM, the cascaded LBM is successfully combined with a multiphase method, and shown to perform as well as the more established MRT method. The cascaded LBM is found to be a considerably improved approach to the simulation of multiphase flow over the LBGK, significantly increasing the stability range of both density ratio and Reynolds number. Additionally the importance of including third order velocity terms in the equilibria of both the cascaded and MRT methods is discussed.

1. Introduction

The lattice Boltzmann method (LBM) is a rapidly developing approach to computational fluid dynamics (CFD). It has been successfully applied to a variety of problems, including (but not limited to) turbulence, micro flows, flows through porous media, magnetohydrodynamics and both multiphase and multi-component systems (see e.g. [1–3] and references therein). Instead of solving the macroscopic Navier–Stokes equations as in traditional CFD, the LBM works on the mesoscopic scale, solving a discretised Boltzmann equation, designed to recover the Navier–Stokes equations in the macroscopic limit. As the LBM works with particle distribution functions, complex macroscopic fluid behaviors which occur as a result of particle interactions, such as phase separation, can be easily included. As interfaces between high and low density phases arise naturally, no interface tracking is required, representing a significant advantage over traditional CFD methods for multiphase flows.

A number of methods for including multiphase behavior into the LBM have been proposed, including the free-energy models [4–6], those based on the kinetic theory of dense fluids [7–9], and the interaction potential models [10–12] which are used here. Originally proposed by Shan and Chen [10] these models calculate a force through a local interaction

* Corresponding author. Tel.: +44 7725 349083.
E-mail address: djlb1e08@soton.ac.uk (D. Lycett-Brown).

0898-1221/$ – see front matter © 2013 The Authors. Published by Elsevier Ltd. All rights reserved.
http://dx.doi.org/10.1016/j.camwa.2013.08.033

potential, which then modifies the equilibrium distribution functions. Despite the success of the multiphase LBM, simulating flows with both a high density ratio between the liquid and gas phases and low viscosity remains challenging, a major problem being the well known formation of spurious velocities around curved interfaces. A number of improvements to the interaction potential model have been proposed, and can be divided into two categories; those that modify the force calculation, such as increasing the order of isotropy [13] or modifying the equation of state [14], and those that improve the incorporation of the force into the equilibrium distribution functions, such as the exact difference method (EDM) [15], and the method by Guo et al. [16]. Lee and Fischer [17] have recently introduced a new model which recasts the force calculation from the pressure form used in the interaction potential models, to a potential form, so as to eliminate discretization errors responsible for the spurious velocities. The scheme is shown to remove spurious velocities from interfaces at equilibrium, however compromises conservation of mass and momentum [18].

In its simplest form the LBM uses a single relaxation time Bhatnagar–Gross–Krook (BGK) collision operator. It has been extensively shown in the single phase case that a significant improvement in attainable Reynolds number can be obtained through the use of a multiple relaxation time collision operator [19–22]. Instead of relaxing particle distribution functions towards their equilibrium distribution functions, a transformation is made into moment space, where individual moments can be relaxed independently, and the relaxation rates of higher order moments can be used to increase stability. Attempts have been made to apply this to the various multiphase schemes, leading in some cases to an increase in attainable Reynolds number [23–27]. A decrease in spurious velocities has also been observed. Recently Geier et al. [28] proposed the cascaded LBM, in which the collision operator relaxes moments in a co-moving reference frame, and showed improvements over results obtained using the MRT collision operator. Here, this cascaded LBM is applied to the multiphase case, with results compared to an MRT implementation. The EDM is used (in both cases), as this gives significant improvement over the original Shan–Chen implementation of the interaction potential model, and does not modify the collision operator (as is the case in the method of Guo et al.).

Here an alternative derivation of the cascaded LBM is presented in Section 2, and the MRT method used for comparison is described in Section 3. The multiphase method using the EDM, is introduced in Section 4. Results and comparisons are then given in Section 5, and conclusions drawn.

2. Cascaded LBM

Although the MRT method significantly enhances stability over the LBGK method as viscosity decreases, it still becomes unstable for sufficiently low viscosities. Geier et al. offered an explanation for this instability, and derived the cascaded LBM in an attempt to overcome it [28]. The two main problems with the MRT method were identified as insufficient Galilean invariance, and a so-called 'crosstalk' between moments. The Galilean invariance arises as a result of relaxing raw moments, defined in the reference frame of a fixed lattice, and can be overcome by instead relaxing central moments, defined in a reference frame moving with the fluid. These central moments can be expressed in terms of raw moments, with central moments of a certain order only containing terms of raw moments of that order and below. Relaxing a raw moment therefore effects higher order central moments, and it is this crosstalk between central moments that is suggested as a source of instability. This is overcome through relaxing moments in a cascade from lowest to highest order moment, the effect of the relaxation of a raw moment on a higher order central moment being known and removed before that higher moment is itself relaxed.

Here we follow a slightly different derivation to that given by Geier et al. and begin with the raw moment representation of populations (see e.g. [19]). These are then translated into their central moment form, before each central moment is independently relaxed. The two-dimensional, nine velocity lattice is used, with velocities $v_{(i,j)} = (v_{(i)}, v_{(j)})$, constructed as the tensor product of the velocities from the sets of two one-dimensional, three velocity lattices, with $v_{(i)} = i$, where $i = 0, \pm 1$. Moments of this product lattice can be written as [29]

$$\rho M_{pq} = \langle f_{(i,j)} v_{(i)}^p v_{(j)}^q \rangle, \quad p, q \in \{0, 1, 2\}, \tag{1}$$

where $\langle \ldots \rangle$ represents summation over all of the velocity indices. In this notation $M_{00} = 1$ is the normalized density, and M_{10} and M_{01} the x and y velocities (u_x and u_y) respectively. We define the trace of the pressure tensor, T, and the normal stress difference, N, (both at unity density) as

$$T = M_{20} + M_{02}, \qquad N = M_{20} - M_{02}. \tag{2}$$

$\Pi_{xy} = M_{11}$ is the off diagonal element of the pressure tensor (at unit density), and $Q_{yxx} = M_{21}$, $Q_{xyy} = M_{12}$ and $A = M_{22}$ are the third and fourth order moments. Populations can be expressed in terms of these moments as:

$$\begin{aligned}
f_{(0,0)} &= \rho\,[1 - T + A]\,, \\
f_{(\sigma,0)} &= \frac{1}{2}\rho\left[\frac{1}{2}(T + N) + \sigma u_x - \sigma Q_{xyy} - A\right], \\
f_{(0,\lambda)} &= \frac{1}{2}\rho\left[\frac{1}{2}(T - N) + \lambda u_y - \lambda Q_{yxx} - A\right], \\
f_{(\sigma,\lambda)} &= \frac{1}{4}\rho\left[A + \sigma\lambda\Pi_{xy} + \sigma Q_{xyy} + \lambda Q_{yxx}\right],
\end{aligned} \tag{3}$$

where $\sigma, \lambda = \{-1, 1\}$. Central moments are defined as in Geier et al. [28], as:

$$\rho\tilde{M}_{pq} = \left\langle (v_{(i)} - u_x)^p (v_{(j)} - u_y)^q f_{(i,j)} \right\rangle. \tag{4}$$

After some algebra, each of the raw moments can be expressed in terms of central moments,

$$\begin{aligned}
\Pi_{xy} &= \tilde{\Pi}_{xy} + u_x u_y, \\
N &= \tilde{N} + (u_x^2 - u_y^2), \\
T &= \tilde{T} + u^2, \\
Q_{xyy} &= \tilde{Q}_{xyy} + 2u_y\tilde{\Pi}_{xy} - \frac{1}{2}u_x\tilde{N} + \frac{1}{2}u_x\tilde{T} + u_x u_y^2, \\
Q_{yxx} &= \tilde{Q}_{yxx} + 2u_x\tilde{\Pi}_{xy} + \frac{1}{2}u_y\tilde{N} + \frac{1}{2}u_y\tilde{T} + u_y u_x^2, \\
A &= \tilde{A} + 2u_x\tilde{Q}_{xyy} + 2u_y\tilde{Q}_{yxx} + 4u_x u_y\tilde{\Pi}_{xy} + \frac{1}{2}u^2\tilde{T} - \frac{1}{2}\left(u_x^2 - u_y^2\right)\tilde{N} + u_x^2 u_y^2,
\end{aligned} \tag{5}$$

and these can be substituted into Eq. (3), to give

$$\begin{aligned}
f_{(0,0)} &= \rho\left[1 + u_x^2u_y^2 - u^2 + 4u_xu_y\tilde{\Pi}_{xy} - \left(\frac{u_x^2 - u_y^2}{2}\right)\tilde{N} + \left(\frac{u^2 - 2}{2}\right)\tilde{T} + 2u_x\tilde{Q}_{xyy} + 2u_y\tilde{Q}_{yxx} + \tilde{A}\right], \\
f_{(\sigma,0)} &= \frac{\rho}{2}\left[u_x^2 + \sigma u_x\left(1 - u_y^2\right) - u_x^2u_y^2 - \left(2\sigma u_y + 4u_xu_y\right)\tilde{\Pi}_{xy} + \left(\frac{1 + \sigma u_x + u_x^2 - u_y^2}{2}\right)\tilde{N}\right. \\
&\quad \left. + \left(\frac{1 - \sigma u_x - u^2}{2}\right)\tilde{T} - \left(\sigma + 2u_x\right)\tilde{Q}_{xyy} - 2u_y\tilde{Q}_{yxx} - \tilde{A}\right], \\
f_{(0,\lambda)} &= \frac{\rho}{2}\left[u_y^2 + \lambda u_y\left(1 - u_x^2\right) - u_x^2u_y^2 - \left(2\lambda u_y + 4u_xu_y\right)\tilde{\Pi}_{xy} + \left(\frac{-1 - \lambda u_y + u_x^2 - u_y^2}{2}\right)\tilde{N}\right. \\
&\quad \left. + \left(\frac{1 - \lambda u_y - u^2}{2}\right)\tilde{T} - \left(\lambda + 2u_y\right)\tilde{Q}_{yxx} - 2u_x\tilde{Q}_{xyy} - \tilde{A}\right], \\
f_{(\sigma,\lambda)} &= \frac{\rho}{4}\left[\sigma\lambda u_xu_y + \sigma u_xu_y^2 + \lambda u_yu_x^2 + u_x^2u_y^2 + \left(4u_xu_y + \sigma\lambda + 2\sigma u_y + 2\lambda u_x\right)\tilde{\Pi}_{xy}\right. \\
&\quad \left. + \left(\frac{-u_x^2 + u_y^2 - \sigma u_x + \lambda u_y}{2}\right)\tilde{N} + \left(\frac{u^2 + \sigma u_x + \lambda u_y}{2}\right)\tilde{T} + \left(\sigma + 2u_x\right)\tilde{Q}_{xyy} + \left(\lambda + 2u_y\right)\tilde{Q}_{yxx} + \tilde{A}\right].
\end{aligned} \tag{6}$$

With the populations written in this form, a collision operator with independent relaxation rates for each central moment can be derived. The LBM is written as

$$f_{(i,j)}\left(\boldsymbol{x} + \boldsymbol{v}_{(i,j)}, t + 1\right) = f^*_{(i,j)}(\boldsymbol{x}, t), \tag{7}$$

where collisions are written in the familiar form

$$f^*_{(i,j)} = (1 - \omega)f_{(i,j)} + \omega f^{eq}_{(i,j)}. \tag{8}$$

Using the form of $f_{(i,j)}$ in Eq. (6), for example for $f^*_{(0,0)}$ this becomes

$$\begin{aligned}
f^*_{(0,0)} &= \rho\left[1 - u^2 + u_x^2u_y^2 + 4u_xu_y\left((1 - \omega)\tilde{\Pi}_{xy} + \omega\tilde{\Pi}^{eq}_{xy}\right)\right. \\
&\quad + \left(\frac{-u_x^2 + u_y^2}{2}\right)\left((1 - \omega)\tilde{N} + \omega\tilde{N}^{eq}\right) + \left(\frac{u^2 - 2}{2}\right)\left((1 - \omega)\tilde{T} + \omega\tilde{T}^{eq}\right) \\
&\quad \left. + 2u_x\left((1 - \omega)\tilde{Q}_{xyy} + \omega\tilde{Q}^{eq}_{xyy}\right) + 2u_y\left((1 - \omega)\tilde{Q}_{yxx} + \omega\tilde{Q}^{eq}_{yxx}\right) + \left((1 - \omega)\tilde{A} + \omega\tilde{A}^{eq}\right)\right],
\end{aligned} \tag{9}$$

where the equilibrium values for the moments are given by [29]

$$\tilde{\Pi}^{eq}_{xy} = \tilde{N}^{eq} = \tilde{Q}^{eq}_{xyy} = \tilde{Q}^{eq}_{yxx} = 0, \qquad \tilde{T}^{eq} = 2c_s^2, \qquad \tilde{A}^{eq} = c_s^4, \tag{10}$$

where $c_s^2 = 1/3$ is the speed of sound squared. The relaxation rate for the trace of the pressure tensor, T, can be replaced by ω_b, relating to the bulk viscosity, and the relaxation rates for the third and fourth order moments replaced by ω_3 and ω_4 respectively. This allows the bulk viscosity to be set independently of the kinematic viscosity, ν, and the higher order moments to be relaxed independently. Using the equilibrium values of the moments, this leads to:

$$
\begin{aligned}
f^*_{(0,0)} &= \rho\left[1 - u^2 + 4u_xu_y\tilde{\Pi}^*_{xy} - \left(\frac{u_x^2 - u_y^2}{2}\right)\tilde{N}^* + \left(\frac{u^2-2}{2}\right)\tilde{T}^* + 2u_x\tilde{Q}^*_{xyy} + 2u_y\tilde{Q}^*_{yxx} + \tilde{A}^*\right],\\
f^*_{(\sigma,0)} &= \frac{\rho}{2}\left[u_x^2 + \sigma u_x\left(1-u_y^2\right) - \left(2\sigma u_y + 4u_xu_y\right)\tilde{\Pi}^*_{xy} + \left(\frac{1+\sigma u_x + u_x^2 - u_y^2}{2}\right)\tilde{N}^*\right.\\
&\quad \left. + \left(\frac{1-\sigma u_x - u^2}{2}\right)\tilde{T}^* - \left(\sigma + 2u_x\right)\tilde{Q}^*_{xyy} - 2u_y\tilde{Q}^*_{yxx} - \tilde{A}^*\right],\\
f^*_{(0,\lambda)} &= \frac{\rho}{2}\left[u_y^2 + \lambda u_y\left(1-u_x^2\right) - \left(2\lambda u_y + 4u_xu_y\right)\tilde{\Pi}^*_{xy} + \left(\frac{-1-\lambda u_y + u_x^2 - u_y^2}{2}\right)\tilde{N}^*\right.\\
&\quad \left. + \left(\frac{1-\lambda u_y - u^2}{2}\right)\tilde{T}^* - \left(\lambda + 2u_y\right)\tilde{Q}^*_{yxx} - 2u_x\tilde{Q}^*_{xyy} - \tilde{A}^*\right],\\
f^*_{(\sigma,\lambda)} &= \frac{\rho}{4}\left[\sigma\lambda u_xu_y + \sigma u_xu_y^2 + \lambda u_yu_x^2 + \left(4u_xu_y + \sigma\lambda + 2\sigma u_y + 2\lambda u_x\right)\tilde{\Pi}^*_{xy}\right.\\
&\quad \left. + \left(\frac{-u_x^2 + u_y^2 - \sigma u_x + \lambda u_y}{2}\right)\tilde{N}^* + \left(\frac{u^2 + \sigma u_x + \lambda u_y}{2}\right)\tilde{T}^* + \left(\sigma + 2u_x\right)\tilde{Q}^*_{xyy} + \left(\lambda + 2u_y\right)\tilde{Q}^*_{yxx} + \tilde{A}^*\right],
\end{aligned}
\tag{11}
$$

where fourth order velocity terms have been dropped, and

$$
\begin{aligned}
\tilde{\Pi}^*_{xy} &= (1-\omega)\,\tilde{\Pi}_{xy},\\
\tilde{N}^* &= (1-\omega)\,\tilde{N},\\
\tilde{T}^* &= (1-\omega_b)\,\tilde{T} + \frac{2}{3}\omega_b,\\
\tilde{Q}^*_{xyy} &= (1-\omega_3)\,\tilde{Q}_{xyy},\\
\tilde{Q}^*_{yxx} &= (1-\omega_3)\,\tilde{Q}_{yxx},\\
\tilde{A}^* &= (1-\omega_4)\,\tilde{A} + \frac{1}{9}\omega_4.
\end{aligned}
\tag{12}
$$

Under the constraint of $\omega_b = \omega_3 = \omega_4 = \omega$, this exactly recovers the BGK form of the collision operator. Using the Chapman–Enskog multi-scales expansion it can be shown that this scheme recovers the isothermal Navier–Stokes equations at reference temperature $T_0 = c_s^2$:

$$
\begin{aligned}
&\frac{\partial\rho}{\partial t} + \nabla\cdot(\rho\boldsymbol{u}) = 0,\\
&\frac{\partial}{\partial t}(\rho\boldsymbol{u}) + \nabla\cdot(\rho\boldsymbol{u}\boldsymbol{u}) + \nabla p = \nabla\cdot\boldsymbol{\tau},
\end{aligned}
\tag{13}
$$

where

$$
\tau_{\alpha\beta} = \rho\nu\left(\frac{\partial u_\beta}{\partial x_\alpha} + \frac{\partial u_\alpha}{\partial x_\beta} - \delta_{\alpha\beta}\nabla\cdot\boldsymbol{u}\right) + \rho\xi\delta_{\alpha\beta}\nabla\cdot\boldsymbol{u},
\tag{14}
$$

and

$$
\nu = \left(\frac{1}{\omega} - \frac{1}{2}\right)c_s^2, \qquad \xi = \left(\frac{1}{\omega_b} - \frac{1}{2}\right)c_s^2,
\tag{15}
$$

are the kinematic and bulk viscosities.

The form presented here is equivalent to the cascaded LBM given in Geier et al. [28], and results for increase in stability in the single phase case are therefore found to be the same as those given therein.

3. MRT method

For comparison an MRT method is used [19–22]. This involves transformation from the population basis to a moment basis in which moments are relaxed, and in the original formulation the transformation between these bases was achieved via a transformation matrix. The MRT method can also be derived by revisiting the derivation of the cascaded LBM given above and simply removing the transformation step from the raw moment basis to the central moment basis, as is done in the following. The matrix form is also presented for completeness, although obviously the two different forms of the equations are equivalent. In the cascaded method post-collision states are written in terms of central moments relaxed towards their equilibria, in the MRT method they are written as raw moments relaxed towards their corresponding equilibria. In the equivalent to Eq. (9), the post-collision state $f^*_{0,0}$ in the LBGK case can be rewritten as

$$f^*_{(0,0)} = \rho\left[1 - \left((1-\omega)\,\tilde{T} + \omega\tilde{T}^{eq}\right) + \left((1-\omega)\,\tilde{A} + \omega\tilde{A}^{eq}\right)\right]. \tag{16}$$

In this form relaxation rates can again be replaced to allow bulk viscosity to be varied independently and the third and fourth order moments relaxed separately. The full set of post-collision populations is then

$$\begin{aligned}
f^*_{(0,0)} &= \rho\left[1 - T^* + A^*\right],\\
f^*_{(\sigma,0)} &= \frac{1}{2}\rho\left[\frac{1}{2}(T^* + N^*) + \sigma u_x - \sigma Q^*_{xyy} - A^*\right],\\
f^*_{(0,\lambda)} &= \frac{1}{2}\rho\left[\frac{1}{2}(T^* - N^*) + \lambda u_y - \lambda Q^*_{yxx} - A^*\right],\\
f^*_{(\sigma,\lambda)} &= \frac{1}{4}\rho\left[A^* + \sigma\lambda\Pi^*_{xy} + \sigma Q^*_{xyy} + \lambda Q^*_{yxx}\right],
\end{aligned} \tag{17}$$

where post-collision moments are

$$\begin{aligned}
\Pi^*_{xy} &= (1-\omega)\,\Pi_{xy} + \omega u_x u_y,\\
N^* &= (1-\omega)\,N + \omega\left(u_x^2 - u_y^2\right),\\
T^* &= (1-\omega_b)\,T + \omega_b\left(2c_s^2 + u^2\right),\\
Q^*_{xyy} &= \left(1-\omega_3'\right)Q_{xyy} + \omega_3' u_x\left(c_s^2 + u_y^2\right),\\
Q^*_{yxx} &= \left(1-\omega_3'\right)Q_{yxx} + \omega_3' u_y\left(c_s^2 + u_x^2\right),\\
A^* &= \left(1-\omega_4'\right)A + \omega_4'\left(c_s^2 + u_y^2\right)\left(c_s^2 + u_x^2\right).
\end{aligned} \tag{18}$$

Equilibrium values have been inserted and primes are used to distinguish raw moment relaxation rates from central moment relaxation rates.

To express this in terms of matrix transformations in general the LBM can be written as

$$f_i(\boldsymbol{x} + \boldsymbol{v}_i, t+1) - f_i(\boldsymbol{x}, t) = -\sum_j \Lambda_{ij}\left(f_j(\boldsymbol{x}, t) - f_j^{eq}(\boldsymbol{x}, t)\right), \tag{19}$$

where for the specific case of the LBGK model the collision matrix Λ_{ij} is given by

$$\Lambda_{ij} = \frac{1}{\tau}\delta_{ij}, \tag{20}$$

where $\tau = 1/\omega$. In general, however, this is a full matrix, and solving Eq. (19) becomes complex. Through the use of a transformation matrix, $\boldsymbol{K}$, the collision matrix can be diagonalized. This transformation matrix is chosen such that

$$\boldsymbol{K}\boldsymbol{f} = \boldsymbol{M}, \tag{21}$$

where $\boldsymbol{f}$ is the vector of population distribution functions, and $\boldsymbol{M}$ is the vector of moments,

$$\boldsymbol{M} = \left(\rho, u_x, u_y, \Pi_{xy}, N, T, Q_{xyy}, Q_{yxx}, A\right)^T. \tag{22}$$

It transforms from the basis of populations to that of moments, and is given by

$$\boldsymbol{K} = \begin{pmatrix}
1 & 1 & 1 & 1 & 1 & 1 & 1 & 1 & 1\\
0 & 1 & 0 & -1 & 0 & 1 & -1 & -1 & 1\\
0 & 0 & 1 & 0 & -1 & 1 & 1 & -1 & -1\\
0 & 0 & 0 & 0 & 0 & 1 & -1 & 1 & -1\\
0 & 1 & -1 & 1 & -1 & 0 & 0 & 0 & 0\\
0 & 1 & 1 & 1 & 1 & 2 & 2 & 2 & 2\\
0 & 0 & 0 & 0 & 0 & 1 & 1 & -1 & -1\\
0 & 0 & 0 & 0 & 0 & 1 & -1 & -1 & 1\\
0 & 0 & 0 & 0 & 0 & 1 & 1 & 1 & 1
\end{pmatrix}. \tag{23}$$

Different transformation matrices have been used in different MRT methods, corresponding to different moment bases, and it is normal to orthogonalize this matrix, for example via the Gram–Schmidt procedure, however this is unnecessary for the present discussion. Using this transformation matrix the MRT method can now be written as

$$f_i(\boldsymbol{x}+\boldsymbol{v}_i, t+1) - f_i(\boldsymbol{x}, t) = -\rho \boldsymbol{K}^{-1}\left(\sum_\beta \hat{\Lambda}_{\alpha\beta}\left(M_\beta(\boldsymbol{x}, t) - M_\beta^{eq}(\boldsymbol{x}, t)\right)\right), \tag{24}$$

where $\boldsymbol{K}^{-1}$ transforms the relaxed moments back into velocity space for the propagation step, and $\hat{\Lambda} = \boldsymbol{K}\Lambda\boldsymbol{K}^{-1}$ is a diagonal matrix,

$$\hat{\Lambda} = \mathrm{diag}\left(1, \omega_b, \omega_4', 1, \omega_3', 1, \omega_3', \omega, \omega\right). \tag{25}$$

It is worth repeating that this is equivalent to the MRT as given by Eqs. (7), (17) and (18). Although different MRT schemes using different bases have been proposed it should be noted that the cascaded LBM cannot be recast in such a way by a linear transformation. However, as discussed by Asinari [30], the cascaded LBM can be cast in matrix form by linearizing the fourth order moment. The Chapman–Enskog procedure can be applied to this MRT scheme, and while this is not done here, the result is the same as for the cascaded LBM, with shear and bulk viscosities given by Eq. (15).

The MRT and cascaded methods are closely related, involving propagation of distribution functions in velocity space, followed by a transformation into moment space (using either raw moments in the MRT method, or central moments in the cascaded method), relaxation in this moment space, and transformation back to velocity space. As shown in Geier et al. [31], the third order terms in velocity are required to maintain Galilean invariance. For the decay of a sinusoidal shear wave, with amplitude in the y-direction, it was shown that a superimposed x-velocity reduced the measured viscosity by a factor proportional to u_x^2, unless the third order terms were included. For fair comparison, these terms are also included in the MRT method, and their effects on the multiphase results are discussed in Section 5.

4. Exact difference method

The original Shan–Chen method for multiphase flow calculated a force from a density dependent interaction potential, and introduced this force into the LBM through modifying the momentum in the equilibrium distribution function. It is well known that including the forcing term in this way leads to a scheme which is unstable for values of ω much higher than 1. A number of improvements to this method have been suggested, including the method of explicit derivatives, as used in the multiphase schemes derived from the kinetic theory of dense fluids [7–9], the method of Guo et al. [16] which takes into account discrete lattice effects, and the EDM. These schemes differ in the second order and higher moments of the forcing term, and as we are concerned here with relaxing higher order moments it is important to choose a method which introduces the lowest errors in the higher order terms. To compare each of the different schemes they can all be written in the general form

$$f_{(i,j)}(\boldsymbol{x}+\boldsymbol{v}_{(i,j)}, t+1) - f_{(i,j)}(\boldsymbol{x}, t) = \Omega + F_{(i,j)}, \tag{26}$$

where Ω is a generic collision operator, and $F_{(i,j)}$ has moments

$$\sum F_{(i,j)} = 0, \tag{27}$$

$$\sum \boldsymbol{v}_{(i,j)} F_{(i,j)} = \boldsymbol{F}, \tag{28}$$

$$\sum \boldsymbol{v}_{(i,j)}\boldsymbol{v}_{(i,j)} F_{(i,j)} = \boldsymbol{\Psi}. \tag{29}$$

Here the general term $\boldsymbol{\Psi}$ has been introduced as the second order moment. While this should equal $(\boldsymbol{Fu} + \boldsymbol{uF})$ in the continuous case, in the discrete case it should include additional terms to cancel discretization errors, and differs in each of the different forcing methods. By series expansion of Eq. (26) the momentum equation is derived as

$$\frac{\partial}{\partial t}\left(\rho\hat{\boldsymbol{u}}\right) + \nabla\cdot\left(\rho\hat{\boldsymbol{u}}\hat{\boldsymbol{u}}\right) + \nabla p = \boldsymbol{F} + \nabla\cdot\hat{\boldsymbol{\tau}} + \nabla\cdot\boldsymbol{E}, \tag{30}$$

where $\rho\hat{\boldsymbol{u}} = \rho\boldsymbol{u} + \boldsymbol{F}/2$, $\hat{\boldsymbol{\tau}}$ is given by

$$\hat{\tau}_{\alpha\beta} = \rho\nu\left(\frac{\partial\hat{u}_\beta}{\partial x_\alpha} + \frac{\partial\hat{u}_\alpha}{\partial x_\beta} - \delta_{\alpha\beta}\nabla\cdot\hat{\boldsymbol{u}}\right) + \rho\xi\delta_{\alpha\beta}\nabla\cdot\hat{\boldsymbol{u}}, \tag{31}$$

and $\boldsymbol{E}$ is an error term given by

$$\boldsymbol{E} = \tau\left(\boldsymbol{Fu} + \boldsymbol{uF}\right) - \tau\boldsymbol{\Psi} + \left(\tau - \frac{1}{4}\right)\frac{\boldsymbol{FF}}{\rho}. \tag{32}$$

In the continuous case the second order moment of $F_{(i,j)}$ cancels the first term. Each of the different forcing schemes do this correctly, the leading order difference is in the third term. $\boldsymbol{\Psi}$ should also contain terms that cancel the third term,

however in each scheme the coefficient in front of the $\boldsymbol{FF}$ term differs. The different resulting error terms are discussed below. Additionally, Wagner [32] concluded that as the pressure tensor contains second order derivatives that are large near to interfaces, the usual second order Chapman–Enskog expansion is insufficient to identify them. Using a fifth order Taylor expansion it was shown for a one-dimensional example that the error term should also contain terms proportional to the gradient of the forcing term.

For the Shan–Chen method the error term is given by

$$\boldsymbol{E}^{\mathrm{SC}} = \left(\tau - \tau^2 - \frac{1}{4}\right)\frac{\boldsymbol{FF}}{\rho}. \tag{33}$$

The dependence on τ of this error is responsible for the poor performance of the method as τ is varied. Kupershtokh's derivation of the EDM was one attempt to solve this problem [15]. As in He et al. [7] the $\nabla_{\boldsymbol{v}} f$ term in the Boltzmann equation can be written approximately as

$$\nabla_{\boldsymbol{v}} f \approx \nabla_{\boldsymbol{v}} f^{eq}. \tag{34}$$

As f cannot be expressed in terms of the microscopic velocity, $\boldsymbol{v}$, then $\nabla_{\boldsymbol{v}} f$ cannot be evaluated, however assuming that the main part of f is f^{eq} then the leading part of the gradient of f will be the gradient of f^{eq} and this approximation will be valid. He et al. [7] therefore wrote the forcing term as

$$\boldsymbol{F} \cdot \nabla_{\boldsymbol{v}} f \approx \frac{\boldsymbol{F} \cdot (\boldsymbol{v} - \boldsymbol{u})}{c_s^2} f^{eq}. \tag{35}$$

Kupershtokh noticed that for Galilean invariance the relationship

$$\nabla_{\boldsymbol{v}} f^{eq} = -\nabla_{\boldsymbol{u}} f^{eq} \tag{36}$$

must be true for the Maxwell–Boltzmann equilibrium distribution. Using the mathematical identity

$$\nabla_{\boldsymbol{u}} f^{eq} \frac{\mathrm{d}\boldsymbol{u}}{\mathrm{d}t} = \frac{\mathrm{d}f^{eq}}{\mathrm{d}t} \tag{37}$$

the discretized forcing term can then be expressed as

$$F^{\mathrm{EDM}}_{(i,j)} = f^{eq}_{(i,j)}(\rho, \boldsymbol{u} + \boldsymbol{F}/\rho) - f^{eq}_{(i,j)}(\rho, \boldsymbol{u}). \tag{38}$$

This can be written out explicitly using the expressions for the equilibrium distributions. It is important to note that when discussing results for second and third order terms in the collision operator that this expression is correspondingly truncated at second and third order. From the second order moment of $F^{\mathrm{EDM}}_{(i,j)}$ the error term can be calculated as

$$\boldsymbol{E}^{\mathrm{EDM}} = -\frac{1}{4}\frac{\boldsymbol{FF}}{\rho}. \tag{39}$$

Unlike in the Shan–Chen method the error term is no longer dependent on τ.

Guo et al. derive their scheme so as to eliminate the leading error, therefore the error term is

$$\boldsymbol{E}^{\mathrm{Guo}} = 0. \tag{40}$$

It should be noted that as the scheme of He et al. does not cancel any of the discretization errors, it has errors which are also dependent on τ. However the derivation given in He et al. also uses the trapezoid rule in discretising the force integral. The transformation of the resulting implicit scheme to an explicit scheme can be rewritten in the form of Eq. (26), for which the force term only differs to the scheme of Guo at third order.

Fig. 1 shows plots of the theoretically derived leading order error terms and the measured gas density for the different schemes, for varying τ. The experimental results are in good agreement with the theoretical predictions of the error, for the lack of dependence on τ in both the EDM and Guo method, the equivalence of the Shan–Chen method and the EDM at $\tau = 1$, and the approach of the Shan–Chen method to that of Guo as τ tends to 0.5. Despite the scheme of Guo et al. having zero error from the second order Chapman–Enskog expansion, the results show greater errors in this scheme than in the EDM. This is likely due to the additional error term derived by Wagner [32], which was found to be proportional to the gradient of the forcing term. This will be high around interfaces and could therefore introduce significant error. Further study of this term is not the purpose of the present work, a possible solution is given by Wagner [32] and methods which appear to cancel this error with a tuneable parameter have been developed by Kupershtokh et al. [33] and Li et al. [34], although without specific reference to the error term.

For the present purpose, the EDM is chosen as it gives only a small error which importantly is not dependent on the viscosity. Significantly for the present work, unlike the other methods, the EDM does not modify the collision operator, therefore the effect of the different collision operators on results can be studied. The result in Fig. 1 was repeated for the

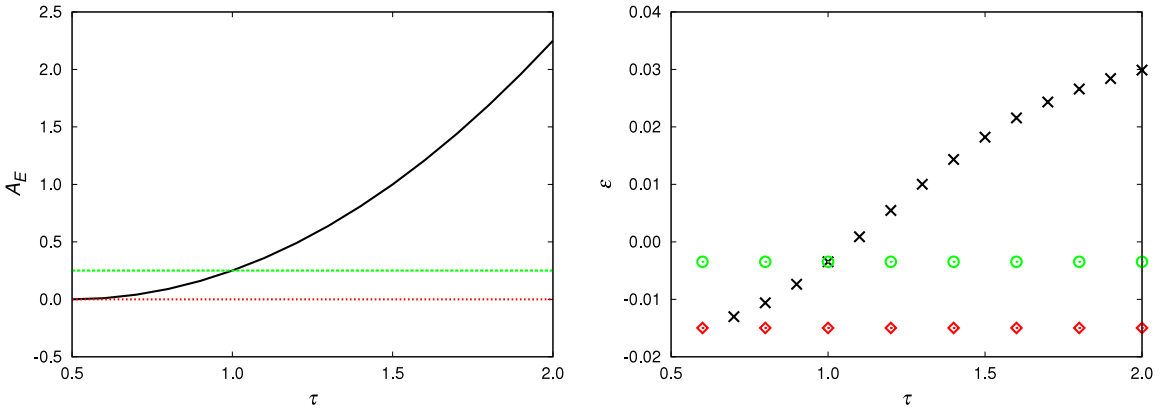

Fig. 1. Comparison between the coefficient of the leading error term, A_E, (left) and the error between the measured gas density and that predicted by the Maxwell rule, ε, (right). The solid black line and black crosses are for the Shan–Chen method [10], $A_E^{\mathrm{SC}} = (1/4 - \tau + \tau^2)$, the dashed green line and green circles are for the EDM [15], $A_E^{\mathrm{EDM}} = 1/4$, and the dotted red line and red diamonds are for the method of Guo [16], $A_E^{\mathrm{Guo}} = 0$.

EDM with varying each of the relaxation parameters of the cascaded method and no effect on the result was observed, therefore the effect of the cascaded LBM on the higher order errors can be evaluated independently of any errors from the EDM. It should be noted that both MRT [35] and cascaded [36] models have been developed which reduce to the forcing scheme of Guo in the LBGK limit.

Following the Shan–Chen model the force term is calculated as

$$\boldsymbol{F} = -G\psi(\boldsymbol{x}) \sum w_{(i,j)} \psi(\boldsymbol{x} + \boldsymbol{v}_{(i,j)}) \boldsymbol{v}_{(i,j)}, \tag{41}$$

where $w_{(0,0)} = 4/9$, $w_{(\sigma,0)} = w_{(0,\lambda)} = 1/9$ and $w_{(\sigma,\lambda)} = 1/36$. This force modifies the equation of state from that of an ideal gas to

$$P = \rho c_s^2 + \frac{G c_s^2}{2} \psi(\boldsymbol{x})^2, \tag{42}$$

where G controls the interaction strength, and ψ is the effective mass, originally give as

$$\psi(\rho) = \rho_0 \left(1 - e^{-\frac{\rho}{\rho_0}}\right). \tag{43}$$

Yuan and Schaefer [14] showed that through rearranging the expression for ψ more realistic equations of state could be introduced, and that this significantly increased the density ratio attainable. The results given in the following section use the Carnahan–Starling equation of state, unless specified otherwise, given by

$$P^{CS} = \rho RT \frac{1 + \frac{b\rho}{4} + \left(\frac{b\rho}{4}\right)^2 - \left(\frac{b\rho}{4}\right)^3}{\left(1 - \frac{b\rho}{4}\right)^3} - a\rho^2, \tag{44}$$

where the constants are set to $R = 1$, $a = 1$ and $b = 4$, in an effective mass given by

$$\psi(\rho) = \sqrt{\frac{2\left(P^{CS} - \rho c_s^2\right)}{G c_s^2}}. \tag{45}$$

With ψ in this form the density ratio is no longer governed by G (now specified to keep the square root acting on a positive number), but by T.

5. Results

5.1. Validation

Comparisons are now made between the results from the cascaded LBM and those of the MRT and LBGK methods. The effect of the third order velocity terms will also be considered. It is first necessary to ensure that adjusting the higher order relaxation rates does not affect the results. Therefore the properties of the system, including density ratio and surface tension, in equilibrium are studied, followed by those of an oscillating droplet. Finally the effects on the spurious velocities are presented.

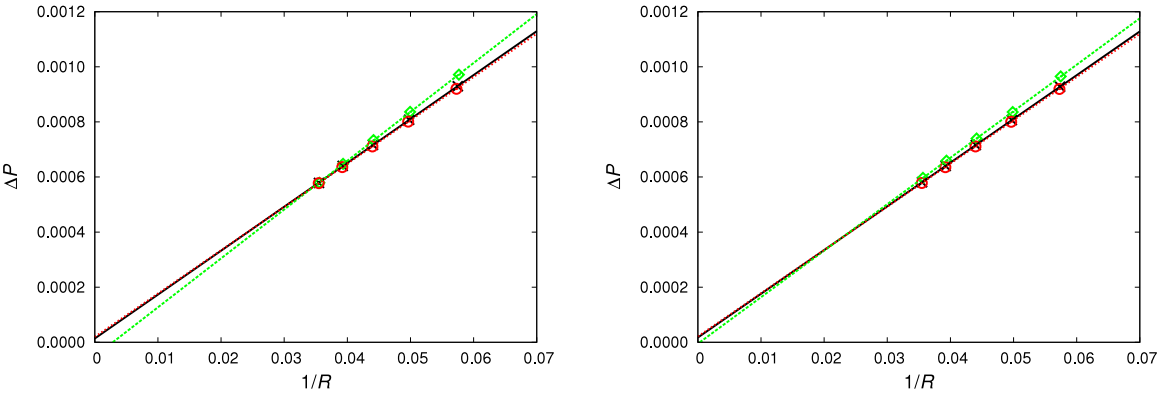

Fig. 2. Laplace law for varying ω_3, at $\omega = 1$, for the LBGK method ($\omega_3 = 1$) (solid black lines), $\omega_3 = 0.2$ (dashed green lines), and $\omega_3 = 1.8$ (dotted red lines). Left and right figures show the results for the second and third order schemes respectively. The measured surface tensions are $\sigma = 0.0159$ for the LBGK method, $\sigma = 0.0177$ for $\omega_3 = 0.2$ and $\sigma = 0.0157$ for $\omega_3 = 1.8$ at second order, and $\sigma = 0.0159$ for the LBGK method, $\sigma = 0.0169$ for $\omega_3 = 0.2$ and $\sigma = 0.0157$ for $\omega_3 = 1.8$ at third order.

Simulations on a 2D, periodic domain of size 5×199, using the Shan–Chen equation of state with $G = -5.4$, were used to evaluate equilibrium properties. The system was initialized with gas in one half of the domain and liquid in the other, and run to equilibrium. It is well known that the Shan–Chen model does not give a constant density ratio for varying viscosity, the EDM resolves this issue, giving a constant density across a range of viscosities. For the MRT method the three relaxation parameters, ω_b, ω_3' and ω_4', were each independently varied between 0.2 and 1.8, at $\omega = 1$, and at $\nu = 0.5$ and 0.0625. Comparing density ratios with those of the LBGK result at $\omega = 1$, results were found to be nearly identical across the range of viscosities and relaxation parameters (in the case of stable simulations), with the largest deviation found to be only 0.03% (for the case of $\omega_b = 1.8$). The same results was found for the cascaded LBM, varying ω_b, ω_3 and ω_4, with the largest variation again being only 0.03% (at $\omega_b = 1.8$). The only significant difference noted between the simulations was the time taken to reach equilibrium. Equilibrium is reached sooner for ω_b close to 0, and later for ω_b near to 2 (and unaffected by changes in the relaxation rates of the third and fourth order moments).

Fixing $\omega = 1$, and varying the density ratio (through varying G), the same setup was used to produce phase diagrams. Again the relaxation parameters were varied, and for both cascaded and MRT methods no visible variation in the phase diagrams were observed, with any differences in density ratio being of the same order as above.

Surface tension can be evaluated using the Laplace law for droplets in equilibrium,

$$\Delta P = \frac{\sigma}{R}, \tag{46}$$

where σ is the surface tension and R the droplet radius. One criticism of the original Shan–Chen model with equation of state in the exponential form was the dependence of surface tension on density ratio, this can however be overcome by tuning the parameters of the Carnahan–Starling equation of state, Eq. (44), or for example by using the grid-refinement method as introduced by Sbragaglia et al. [13]. Here we consider one value of the surface tension by fixing the parameters of the equation of state, as given previously. Droplets of different radii, up to a maximum of $R = 30$, were initiated in the center of a 100×100 domain and simulations run to equilibrium. For this the Carnahan–Starling equation of state was used with $T = 0.063$, giving a density ratio of approximately 100, at both $\omega = 1$ and $\nu = 0.03125$. This was repeated for different values of the relaxation parameters. For the case of $\omega = 1$, varying ω_b or ω_4 across their stable domain produced very little variation in the measured surface tension or offset from the origin, with the greatest deviations in surface tension being less than 0.9% and 0.5% for the case of $\omega_b = 0.4$ and $\omega_4 = 0.2$ respectively. Larger variations were observed when varying ω_3, with the largest being 11.3% at $\omega_3 = 0.2$. Moving from the second order to the third order scheme reduces this maximum variation in surface tension to 6.3% (and has little effect on the ω_b and ω_4 results). The graph of Laplace law for the case of varying ω_3 is given in Fig. 2. A very similar result is observed in the MRT case, with the greatest deviations being 0.9% and 0.1% for the case of $\omega_b = 0.2$ and $\omega_4' = 0.4$ respectively, and 11.9% in the case of $\omega_3' = 0.2$, reducing to 7.6% in the third order scheme. Reducing the viscosity to $\nu = 0.03125$ increases some of these errors slightly. For varying ω_b, ω_3 and ω_4 the maximum deviations in surface tension were found to be 4.0%, 3.7% and 2.6% at $\omega_b = 1.0$, $\omega_3 = 0.4$ and $\omega_4 = 0.8$ for second order, and 4.1%, 3.7% and 2.5% respectively for third order, for the cascaded scheme. Again results are similar using the MRT scheme, for varying ω_b, ω_3' and ω_4' the maximum deviations in surface tension were found to be 2.4%, 5.8% and 1.5% at $\omega_b = 0.8$, $\omega_3' = 0.2$ and $\omega_4' = 1.0$ for second order, and 3.0%, 3.9% and 1.7% respectively for third order.

The Laplace law results show that the relaxation rates can be varied across their whole stability range, without significantly affecting a droplet at equilibrium. Significantly the third and fourth order rates only have a small effect on the result at $\omega = 1$, although this increases for lower viscosity.

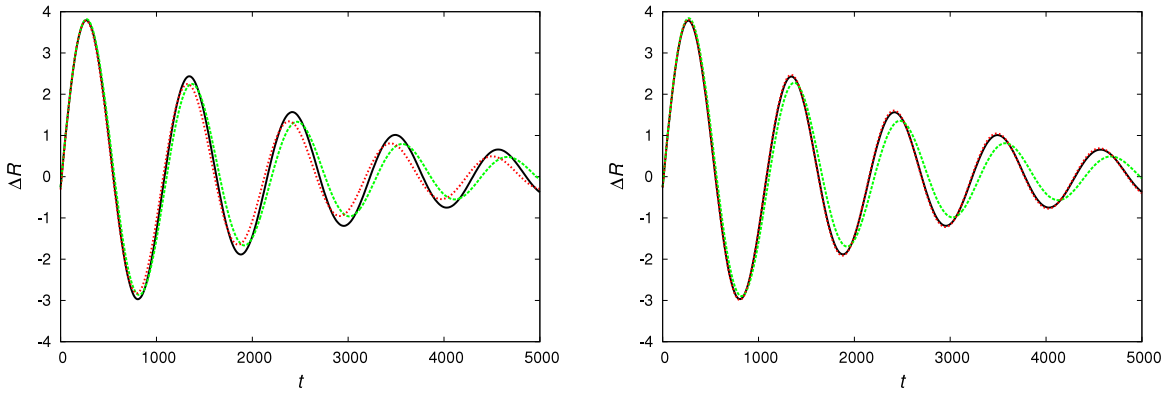

Fig. 3. Droplet oscillations showing the deviation of the interface from its position at equilibrium, ΔR (in lattice units), with time steps, t. Results shown are for $\nu = 0.03125$ for the LBGK method (solid black lines), $\omega_b = 1.0$ (dashed green lines), and $\omega_3 = 0.4$ (dotted red lines). Left and right figures show the results for the second and third order schemes respectively. The measured oscillation periods are $T_o = 1074.2$ for the LBGK method, $T_o = 1097.3$ for $\omega_b = 1.0$, and $T_o = 1059.0$ for $\omega_3 = 0.4$ at second order, and $T_o = 1074.8$ for the LBGK method, $T_o = 1101.3$ for $\omega_b = 1.0$, and $T_o = 1072.8$ for $\omega_3 = 0.4$ at third order.

The case of an oscillating droplet is now considered. The same setup was used, with viscosity set to 0.03125. Once droplets reached equilibrium an initial velocity was applied, given by:

$$\begin{aligned} u_x &= U_0 \frac{x - x_0}{R} \\ u_y &= -2U_0 \frac{y - y_0}{R}, \end{aligned} \tag{47}$$

for droplets centered at (x_0, y_0). Again, this was repeated across the stable domain of each relaxation parameter. Results for the cascaded LBM are shown in Fig. 3. Varying ω_4 produced no visible deviation in result, with a maximum change in period of just 0.1%, and results are therefore not shown. The graphs show the deviation of the droplet interface from its position at equilibrium, along the x-axis. Each case shows the most extreme variation observed within the stable domain of each relaxation parameter, compared with the LBGK solution. For varying ω_b the largest variation in period, as shown in Fig. 3(left), was 2.1% at $\omega_b = 1.0$. This result does not change on moving to third order, as shown in Fig. 3(right). In the case of ω_3, the largest deviation in period from the LBGK result was 1.4% at $\omega_3 = 0.4$ at second order, reducing to just 0.2% for third order. As with the Laplace law, results for the MRT case were very similar, and are therefore not shown. The maximum variations in period were found to be 4.7%, 1.9% and 0.1% at $\omega_b = 0.8$, $\omega_3' = 0.4$ and $\omega_4' = 1.8$, for second order, and 4.9%, 0.3% and 0.1% respectively for third order. As with the cascaded method varying the fourth order moment relaxation rate has virtually no affect on results, with the same being true for the third order moment rate in the third order scheme. A similar result was observed at $\omega = 1$.

5.2. Spurious velocities

As it has been shown that the additional relaxation rates can be varied without having significant effect on the multiphase result, even at low viscosity, these parameters can be used to improve stability without a detrimental effect on accuracy. The following results describe the changes observed in the spurious velocities found around droplets, for varying these relaxation parameters. As well as spurious velocities, another cause of instability in the Shan–Chen LBM has been identified as the higher speed of sound in the liquid phase due to the modified equation of state [37]. Here the focus is on reducing spurious velocities, and both cascaded and MRT models are compared using the same equation of state.

Droplets of radius 20 were set up in the center of a 100×100 domain, with a density ratio of 20 (using $T = 0.073$). At equilibrium the maximum spurious velocity magnitude and average spurious velocity magnitude in the gas phase were recorded. This was repeated for varying all three relaxation parameters simultaneously, with each varied from 0.2 to 1.8 in intervals of 0.2 (a total of 729 simulations). While the maximum spurious velocity, which usually occurs inside the interface, is normally reported, it was observed that this did not always give a good indication of the reduction in spurious velocity throughout the domain, as shown in Fig. 4. Therefore the following results report the reduction in the average spurious velocity in the gas.

Fig. 5 shows results for the minimum value found for the average spurious velocity in the gas around droplets, for a range of viscosities from 1 to 0.001. Results for the cascaded LBM and the MRT method are shown, along with the LBGK case for comparison. Both the cascaded LBM and the MRT method give similar significant reductions in spurious velocity over the LBGK method. This reduction is up to two orders of magnitude for certain viscosities, and taking for example 0.001 as the maximum average spurious velocity in the gas which can be tolerated for a simulation, increases the useable range of low viscosities by roughly two orders of magnitude.

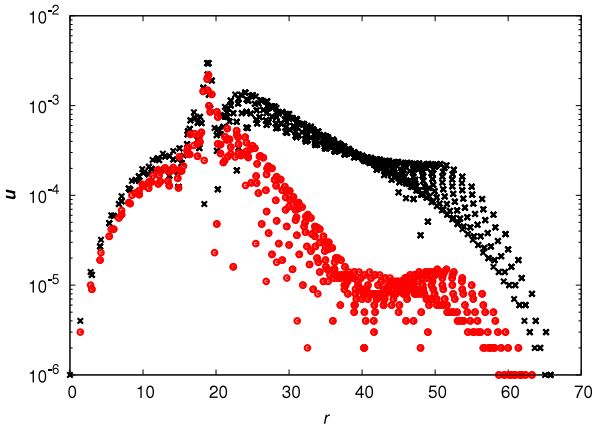

Fig. 4. Magnitude of the spurious velocities around a droplet against the distance from the droplet center, r, for a droplet of radius 20 at $\omega = 1$, for the LBGK method (black crosses) and the cascaded LBM with $\omega_4 = 0.2$ (red circles). A small reduction in maximum spurious velocity (around $r = 20$) is observed, while the reductions in the gas phase ($r > 20$) can be greater than an order of magnitude.

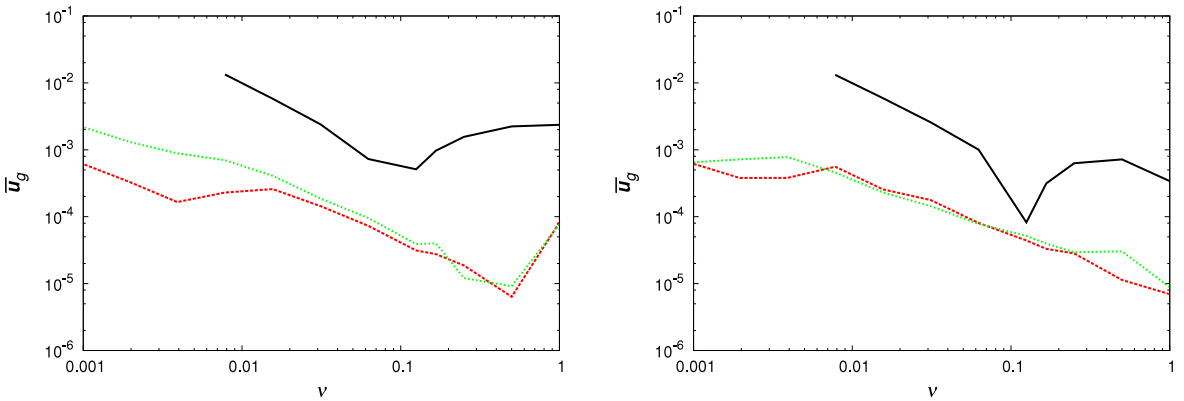

Fig. 5. Minimum average magnitude of the spurious velocities in the gas phase, for varying viscosity at a density ratio of 20. Results are for the LBGK method (solid black line), the MRT method (dotted green line) and the cascaded LBM (dashed red line), for the second order (left figure) and third order (right figure) schemes.

Fixing $\omega = 1$, Fig. 6 shows results for varying density ratio. It can be seen that both the cascaded LBM and the MRT method provide significant reductions in spurious velocities over the LBGK case, with the cascaded LBM giving lower velocities than the MRT method at high density ratios. A two orders of magnitude reduction in spurious velocities over the LBGK method is seen at high density ratios with the cascaded LBM. In the third order case, the improvement over the LBGK method is smaller, due to a large reduction in spurious velocities between the second and third order LBGK models. Results for the cascaded LBM are slightly worse than at second order, bringing them into line with those from the MRT method.

The cascaded LBM has given significant reductions in spurious velocities compared with the LBGK method, across a wide range of viscosities and density ratios, with results similar to or slightly better than those observed with the MRT method. At second order the cascaded method is seen to outperform the MRT method, especially at high density ratios. However in the third order case both the MRT method and the cascaded LBM give very similar improvement over the LBGK method. As the third order term is required to maintain Galilean invariance, and has been shown here in the case of oscillating droplets to be important when varying ω_3, it should be included in the model.

6. Conclusion

It has been shown that an implementation of the cascaded lattice Boltzmann method can significantly reduce the spurious velocities found around curved interfaces in a multiphase system, which uses the Shan–Chen interparticle model to calculate the forcing term. This is achieved through varying the relaxation rates of higher order moments defined in a co-moving reference frame. It has been shown that these relaxation rates can be varied without significant deterioration in the results, and that they can therefore be used to tune the system for lower spurious velocities and improved stability, without compromising the accuracy of the solution. This is in line with the finding of Geier et al. [28] for improved stability over the LBGK method in the single phase case. Additionally it has been shown that third order velocity terms play a significant role and should not be neglected.

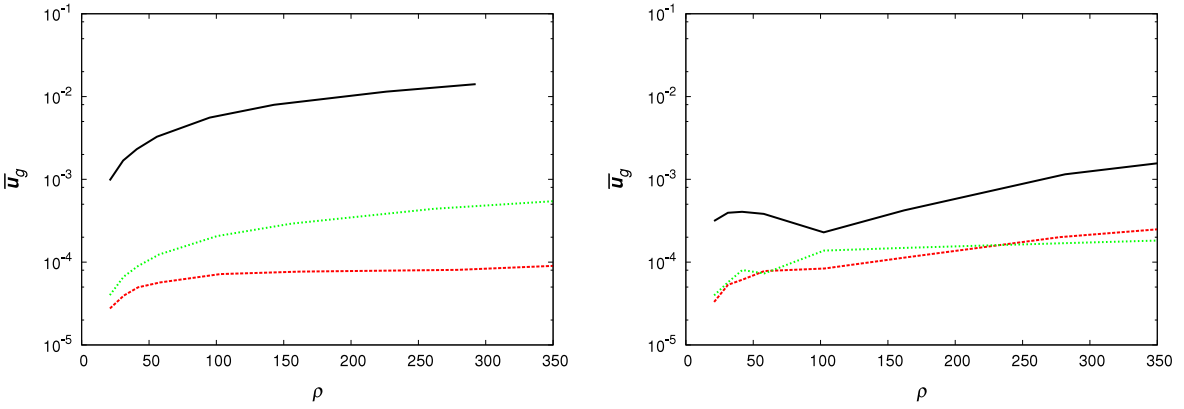

Fig. 6. Minimum average magnitude of the spurious velocities in the gas phase, for varying density ratio at $\omega = 1$. Results are for the LBGK method (solid black line), the MRT method (dotted green line) and the cascaded LBM (dashed red line), for the second order (left figure) and third order (right figure) schemes.

Comparisons were made with an MRT implementation, in both cases the exact difference method was used, so differences between models due to the collision operator alone (and not the multiphase implementation) could be observed. The cascaded model was shown to perform as well as the more established MRT method across a large parameter range. This result, in combination with improvements over the MRT method in the single phase case [28,31], suggests that the cascaded LBM is a valuable addition to the family of lattice Boltzmann models. Finally, the reduction in spurious velocities over the LBGK model extends the useable region of the multiphase LBM in terms of both higher density ratios and lower viscosities, thus bringing the method closer to its goal of simulating the high density ratios and high Reynolds numbers observed in real world systems. A compromise exists between tuning the relaxation parameters for increased stability and reduced spurious velocity, therefore future work should focus on combining the cascaded LBM with other multiphase methods, for example the method of Lee and Fischer [17].

Acknowledgements

We gratefully acknowledge the funding from the Engineering and Physical Sciences Research Council for Grant No. EP/J016381/1 and a HEC Studentship, and insightful discussions with Prof. Ilya Karlin.

References

[1] Y.H. Qian, S. Succi, S.A. Orszag, Recent advances in lattice Boltzmann computing, Annu. Rev. Comput. Phys. 30 (1995) 195.
[2] S. Chen, G.D. Doolen, Lattice Boltzmann method for fluid flows, Annu. Rev. Fluid Mech. 30 (1998) 329.
[3] S. Succi, The Lattice Boltzmann Equation for Fluid Dynamics and Beyond, Oxford University Press, Oxford, 2001.
[4] M.R. Swift, W.R. Osborn, J.M. Yeomans, Lattice Boltzmann simulation of nonideal fluids, Phys. Rev. Lett. 75 (1995) 830.
[5] E. Orlandini, M.R. Swift, J.M. Yeomans, A lattice Boltzmann model of binary-fluid mixtures, Europhys. Lett. 32 (1995) 463.
[6] M.R. Swift, E. Orlandini, W.R. Osborn, J.M. Yeomans, Lattice Boltzmann simulations of liquid–gas and binary fluid systems, Phys. Rev. E 54 (1996) 5041.
[7] X. He, X. Shan, G.D. Doolen, Discrete Boltzmann equation model for nonideal gases, Phys. Rev. E 57 (1998) R13.
[8] X. He, G.D. Doolen, Thermodynamic foundations of kinetic theory and lattice Boltzmann models for multiphase flows, J. Stat. Phys. 107 (2002) 309.
[9] L.-S. Luo, Unified theory of lattice Boltzmann models for nonideal gases, Phys. Rev. Lett. 81 (1998) 1618.
[10] X. Shan, H. Chen, Lattice Boltzmann model for simulating flows with multiple phases and components, Phys. Rev. E 47 (1993) 1815.
[11] X. Shan, H. Chen, Simulation of nonideal gases and liquid–gas phase transitions by the lattice Boltzmann equation, Phys. Rev. E 49 (1994) 2941.
[12] X. Shan, G. Doolen, Multicomponent lattice-Boltzmann model with interparticle interaction, J. Stat. Phys. 81 (1995) 379.
[13] M. Sbragaglia, R. Benzi, L. Biferale, S. Succi, K. Sugiyama, F. Toschi, Generalized lattice Boltzmann method with multirange pseudopotential, Phys. Rev. E 75 (2007) 026702.
[14] P. Yuan, L. Schaefer, Equations of state in a lattice Boltzmann model, Phys. Fluids 18 (2006) 042101.
[15] A.L. Kupershtokh, New method of incorporating a body force term into the lattice Boltzmann equation, in: Proceedings of the 5th International EHD Workshop, University of Poitiers, Poitiers, France, 2004, p. 241.
[16] Z. Guo, C. Zheng, B. Shi, Discrete lattice effects on the forcing term in the lattice Boltzmann method, Phys. Rev. E 65 (2002) 046308.
[17] T. Lee, P.F. Fischer, Eliminating parasitic currents in the lattice Boltzmann equation method for nonideal gases, Phys. Rev. E 74 (2006) 046709.
[18] D. Chiappini, G. Bella, S. Succi, F. Toschi, S. Ubertini, Improved lattice Boltzmann without parasitic currents for Rayleigh–Taylor instability, Commun. Comput. Phys. 7 (2010) 423.
[19] D. d'Humières, Generalized lattice Boltzmann equations, rarefied gas dynamics: theory and simulations, AIAA Prog. Astronaut. Aeronaut. 159 (1992) 450.
[20] P. Lallemand, L.-S. Luo, Theory of the lattice Boltzmann method: dispersion, dissipation, isotropy, Galilean invariance, and stability, Phys. Rev. E 61 (2000) 6546.
[21] D. d'Humières, I. Ginzburg, M. Krafczyk, P. Lallemand, L.-S. Luo, Multiple-relaxation-time lattice Boltzmann models in three dimensions, Phil. Trans. R. Soc. A 360 (2002) 437.
[22] P. Lallemand, L.-S. Luo, Theory of the lattice Boltzmann method: acoustic and thermal properties in two and three dimensions, Phys. Rev. E 68 (2003) 036706.
[23] M.E. McCracken, J. Abraham, Multiple-relaxation-time lattice-Boltzmann model for multiphase flow, Phys. Rev. E 71 (2005) 036701.

[24] J. Tölke, F. Sören, M. Krafczyk, An adaptive scheme using hierarchical grids for lattice Boltzmann multi-phase flow simulations, Comput. & Fluids 35 (2006) 820.
[25] S. Mukherjee, J. Abraham, A pressure-evolution-based multi-relaxation-time high-density-ratio two-phase lattice-Boltzmann model, Comput. & Fluids 36 (2007) 1149.
[26] A. Kuzmin, A.A. Mohamad, S. Succi, Multi-relaxation time lattice Boltzmann model for multiphase flows, Int. J. Mod. Phys. C 19 (2008) 875.
[27] A. Fakhari, M.H. Rahimian, Phase-field modeling by the method of lattice Boltzmann equations, Phys. Rev. E 81 (2010) 036707.
[28] M.C. Geier, A. Greiner, J.G. Korvink, Cascaded digital lattice Boltzmann automata for high Reynolds number flow, Phys. Rev. E 73 (2006) 066705.
[29] I.V. Karlin, P. Asinari, Factorization symmetry in the lattice Boltzmann method, Physica A 389 (2010) 1530.
[30] P. Asinari, Generalized local equilibrium in the cascaded lattice Boltzmann method, Phys. Rev. E 78 (2008) 016701.
[31] M.C. Geier, A. Greiner, J.G. Korvink, Properties of the cascaded lattice Boltzmann automaton, Int. J. Mod. Phys. C 18 (2007) 455.
[32] A.J. Wagner, Thermodynamic consistency of liquid–gas lattice Boltzmann simulations, Phys. Rev. E 74 (2006) 056703.
[33] A.L. Kupershtokh, D.A. Medvedev, D.I. Karpov, On equations of state in a lattice Boltzmann method, Comput. Math. Appl. 58 (2009) 965.
[34] Q. Li, K.H. Luo, X.J. Li, Forcing scheme in pseudopotential lattice Boltzmann model for multiphase flows, Phys. Rev. E 86 (2012) 016709.
[35] Z. Yu, L.-S. Fan, Multirelaxation-time interaction-potential-based lattice Boltzmann model for two-phase flow, Phys. Rev. E 82 (2010) 046708.
[36] K.N. Premnath, S. Banerjee, Incorporating forcing terms in cascaded lattice Boltzmann approach by method of central moments, Phys. Rev. E 80 (2009) 036702.
[37] A.L. Kupershtokh, Criterion of numerical instability of liquid state in LBE simulations, Comput. Math. Appl. 59 (2010) 2236.